Optimization of the Propeller-Driven Propulsion System for a Small UAV

Nuno de Sousa Mendes Moita
nuno.moita@tecnico.ulisboa.pt

Instituto Superior Técnico, Universidade de Lisboa, Portugal

April 2018

Abstract

Integrated in the LEEUAV project, an UAV developed by IDMEC, together with AeroG and INEGI, the objective of this dissertation is to optimize the propeller-driven propulsion system designed and built previously. After some literature review and research about the different existing softwares for propulsion systems analysis, the chosen software was the QPROP. After software selection, a propeller parametrization was made, including the planform and airfoil shape. After running QPROP, some functions were used to evaluate the performance of the propeller, such as thrust, power and thrust coefficient and the propeller efficiency. To perform the experimental tests, three different propellers were chosen to study how the performance varies for different diameters, pitches and motors and to validate the software. Since it was not known accurately which airfoil was used in each propeller, two different airfoils, whose data was obtained using the software XFOIL, were considered. The geometric parameters of the propeller were measured manually. Following the experimental tests and the validation of the software QPROP, a geometry optimization using the software MATLAB®, for cruise and climb, was performed. At the end of this optimization, a system motor+propeller with an higher efficiency for both flight stages was obtained, as desired.
Keywords: Propeller, Optimization, Efficiency, Thrust, Electrical Power

1. Introduction

An Unmanned Aerial Vehicle (UAV) is a type of aircraft which can be controlled from an external source or autonomously by inboard computers, so it has no crew neither passengers. Since the second half of the 19^{th} century, the human race saw a big potential in UAVs development. At the beginning, UAVs were only used for military purposes, such as vigilance and reconnaissance missions. The use of UAVs for civil applications took a longer period of time, due to the high costs and the complexity of civil missions. However, nowadays, the UAVs are used for missions like delivering mail in inaccessible regions, forest fires detection and recognition operations.

The propeller designed in this master thesis will be implemented in the Long Endurance Electrical Unmanned Aerial Vehicle (LEEUAV) project. This project was developed by AeroG at UBI, IDMEC at IST and INEGI at FEUP. The main goal of this project was to develop a cheap and ecological electric UAV, without any carbon dioxide emissions. The aircraft must have the capability to take-off in short airfields, to have an easy construction and maintenance and to be highly flexible to perform several kinds of surveillance missions [1] .

The first objective to achieve is to define a software that performs numerical simulations to obtain the performance data of a given system motor+propeller and to perform a propeller parametrization. Then, it is intended to perform wind tunnel tests to predict the performance of different systems motor+propeller and to perform the validation of the numerical software. The last objective is to build an optimization tool that uses the validated numerical software and determines the optimized geometry and operating conditions to perform in climb and cruise. At the end, it is intended to manufacture the optimized propeller obtained by using the optimization tool.

2. Analytical Propeller Analysis

There are several theories used to perform propeller analysis such as Disk-Actuator theory, Lifting Line theory, Vortex Lattice theory and Panel Method. However, the most common models that are usually used are the Blade Element Theory (BET) and the Blade Element Momentum Theory (BEMT), so, a more detailed description of these theories is shown.

2.1. Blade Element Theory

The Blade Element Theory (BET) was proposed by Drzwieck in 1982 [2] and is a simple and fast method that consists in splitting each blade in independent sections which are analysed based on the local velocities. At each section, a 2D force balance is applied to obtain lift, drag, thrust and torque distributions. A final integration over the entire blade gives the performance characteristics of the blade. The flow is analysed independently on each section assuming there are only axial and angular velocities and there is no induced flow from any other sections. In Figure 1, it is shown the force diagram presented for each cross-section.

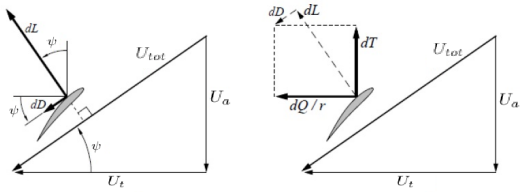

Figure 1: Decomposition of lift and drag into thrust and torque [3]

where U_{tot} is the resultant velocity from the vectorial sum of the axial velocity U_a and the tangential velocity U_t and ψ is the resultant flow angle with respect to the plane of rotation. From figure 1, the total expressions for thrust T and torque Q of the entire blade are obtained and presented as

$$T = \frac{1}{2}\rho B \int_0^R U_{tot}^2 c \left(C_l \cos\psi - C_d \sin\psi\right) dr \quad (1)$$

and

$$Q = \frac{1}{2}\rho \int_0^R U_{tot}^2 c \left(C_l \sin\psi + C_d \cos\psi\right) r dr \,. \quad (2)$$

where B is the number of blades, c is the blade chord distribution and C_l and C_d are the local lift and drag coefficients of the airfoil, respectively. So, this theory allows for the analysis of specific propellers with different geometrics shapes along the blades of a propeller, however, it has an increased complexity and does not account the effect of the induced velocities on the blades, swirl in the slipstream, non-uniform flow, or propeller blockage.

2.2. Blade Element Momentum Theory

The Blade Element Momentum Theory (BEMT) corresponds to an upgrade of the BET where the induced velocities are taken in account. In Figure 2, it is possible to visualize the velocity decomposition of the resultant velocity, U_{tot}.

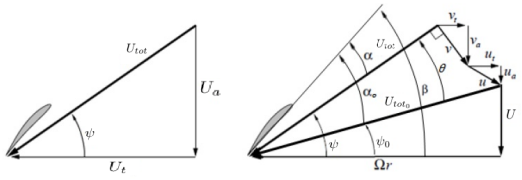

Figure 2: Velocity decomposition and angle definitions [3]

As it can be analysed, the induced velocities u and v are distinguished since v results from the lift generation by the propeller and u represents the externally-induced velocity. At the end, the elemental thrust and torque expressions are obtained as

$$dT = B\rho \left(\frac{2\pi N r}{\cos\psi}\cos\theta\right)^2 c(C_l \cos\psi - C_d \sin\psi) dr \quad (3)$$

and

$$dQ = B\rho \left(\frac{2\pi N r}{\cos\psi}\cos\theta\right)^2 cr(C_l \sin\psi + C_d \cos\psi) dr \,. \quad (4)$$

where N is the motor rotation speed in RPM and θ is the induced angle. Using BEMT, it is possible to obtain the additional detail of considering the induced velocities, however, it increases the complexity of the theory. The only assumption that can limit this theory is that the flow is considered to be bidimensional.

2.3. Propeller Parametrization

To define a propeller, it is necessary to define the three main categories of parameters:

- Planform shape;
- Airfoil characteristics;
- Performance.

To define the planform shape of the propeller, it is necessary to define the propeller diameter D, the propeller chord distribution $c(r)$ and the propeller pitch angle distribution $\beta(r)$.

In relation to the airfoil characteristics, the parameters that are used to define them are important to the software in use to determine the lift curve and the drag polar. To determine the lift curve, the four main parameters that are taken in account are the maximum lift coefficient $C_{l_{max}}$, the minimum lift coefficient $C_{l_{min}}$, the lift coefficient for an angle of attack of zero degrees C_{l_0} and the derivative of the lift coefficient with the angle of attack C_{l_α}. To determine the drag polar, the parameters that are considered are the profile drag coefficient C_{d_0}, the lift coefficient corresponding to the profile drag coefficient $C_{l_{C_{d_0}}}$, the drag coefficient slope C_{l_2}, the

Reynolds number from which all the previous values are obtained Re_{ref} and the Reynolds exponent that adjusts the polar for other Reynolds numbers, Re_{expo}.

In relation to the performance parameters, the first that is necessary to take in account is thrust T. The second performance parameter that must be considered is the thrust coefficient C_T, which is a dimensionless parameter that relates the thrust produced by a propeller with its diameter and rotation velocity, given by

$$C_T = \frac{T}{\rho N^2 D^4} \,. \tag{5}$$

Another performance parameter that must be taken in account is power coefficient C_P, which is a dimensionless parameter that is relates the mechanical power produced by a propeller with its diameter and rotation velocity as

$$C_P = \frac{P_{shaft}}{\rho N^3 D^5} \,. \tag{6}$$

Yet, another parameter that is important is the propeller efficiency η. Since the propeller was pretended to be optimized to reduce the electrical power of the system motor+propeller, this parameter was defined as the ratio between the power that a propeller can use and the electrical power P supplied to the system,

$$\eta = \frac{TU}{P} \,. \tag{7}$$

where P is given by:

$$P = V^* I \,. \tag{8}$$

where V^* is the input voltage of the motor and and I is the current consumed by the motor.

Usually, to analyse the variation of these dimensionless parameters, a parameter called advance ratio, J, is used. This is also a dimensionless parameter, that relates the velocity with the rotation velocity and the diameter of a propeller,

$$J = \frac{U}{ND} \,. \tag{9}$$

3. Numerical Propeller Analysis

In this section, the way each software works is described and consequently it is decided which one will be implemented to study the propeller performance and for the optimization to be conducted in subsequent work.

3.1. Software Description and Implementation

The first software that was studied was the AKPD/AKPA. This software was developed by State Marine Technical University (SMTU), together with Marintek [4] and has a design algorithm based on a non-linear surface theory while the propeller analysis is performed with the Blade Element Theory. However, this software can not be used due to the fact of not being available commercially, since only SMTU and Marintek are allowed to use it.

Secondly, the possibility of using JavaProp was studied. JavaProp [5] is a software created by Martin Hepperle that uses BEMT to perform the propeller analysis and is based on an inverse design module which means that the user starts by specifying basic parameters and a geometry of an optimum propeller is automatically produced. However, it only enables the analysis of optimised propellers and does not account with the motor effect. As such, this software was not used.

The last software that was studied was QPROP [3] which is an analysis program with the ability to predict the propulsive performance using a given combination of motor+propeller. To execute the software there are two main files that are necessary: the motor file, where the motor parameters are defined and the propeller file, where the planform shape and airfoil parameters are defined. The possibility of varying all the parameters allows the software to test all kind of propellers. By using this program, it is just necessary to take in account the conversion of the C_T and C_P values to the units defined in the propeller parametrization. As such, the conversions are performed such that

$$C_T = \frac{\pi^3}{8} C_{T_1} \tag{10}$$

and

$$C_P = \frac{\pi^4}{8} C_{P_1} \,. \tag{11}$$

This software was chosen to be used in the propeller analysis and design framework due to provide all the desirable outputs to perform the analysis, to be the simplest one to use since MATLAB® has the capability to execute external software and to the fact of being the only software that considers the entire system motor+propeller.

4. Experimental Facility

4.1. Electrical Motors

The motors used in this thesis are DC brushless electrical motors which are devices that convert electrical power into mechanical power which assures the rotation of the motor shaft. The two motors used were the OS-3810-1050 and the OS-5020-490 [6], whose characteristics are presented in Table 1, where I_0 is the zero-load current, I_{max} is the maximum current supported by the motor, η_{max} is the maximum efficiency the motor can reach, K_v is the motor constant and R is the internal resistance of the motor.

Motor	Shaft diameter [mm]	V^* [V]	I_{max} [A]	I_0 [A]	η_{max} [%]	K_v [RPM/V]	R [$m\Omega$]
OS-3810-1050	5	12.5	30	1.1	85	1050	51.3
OS-5020-490	6	21.0	68	1.5	85	490	23

Table 1: Characteristics of the electric motors

4.2. Propellers

In this work, three different propellers were analysed. The first propeller to be analysed was an APC 13"×8". This designation means that the propeller has a diameter of 13 inches and has a pitch of 8 inches. The other two propellers to be analysed are an APC 16"×8" and a APC 16"×10". By choosing these three propellers, it was possible to compare the performance of a propeller by varying the diameter and the pitch. Since different propellers were to be tested, it was important to choose the most adequate motor for each one to obtain the highest value of efficiency possible. For the APC 13"×8", the two available brushless electrical motors were used to compare the performance between them. For the APC 16"×8" and the APC 16"×10", the motor used was the OS-5020-490.

Due to the non-existence of geometry details of any of the propellers to be tested, it was necessary to find a way to measure their planform shape. The first method that was used consists in performing a manual measurement. To perform the measurements, the blade was placed in a glass surface to define a referential and to avoid as much as possible some uncertainties. After splitting the blade in several equal sections using white ink and a tissue line, the heights h_1 and h_2 of each section were measured with using a calliper with a scale of 1 ± 0.05 mm. The blade was then removed from the surface and the chord of each section and the blade radius were measured. A scheme of the previous explanation is presented in Figure 3.

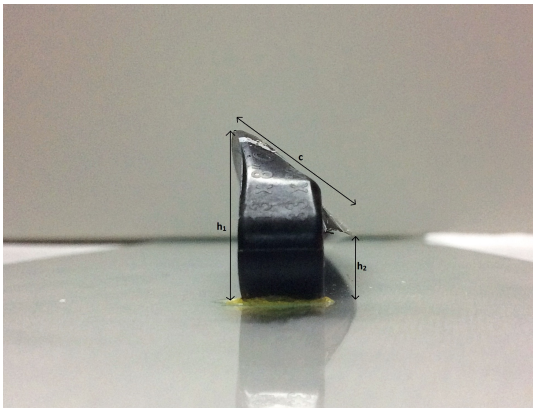

Figure 3: Scheme of the measurement procedure of the blade

As it can be seen in Figure 3, by measuring the heights h_1, h_2 and the chord c, it was possible to determine the distribution of β and of the chord along the blade, for each section k, as

$$\beta_k = \arcsin \frac{h_{1_k} - h_{2_k}}{c_k} \, . \tag{12}$$

The second method was a 3D scanning of the planform shape to improve the accuracy of the results. This method is performed by handling a laser scanner that uses reflective markers to position the object in space, using a computer and an appropriated software to allow the data acquisiton. The device used is the $ZScanner^{TM}$ 700 together with the software $ZScan^{TM}$, whose specifications are presented in [7]. The procedure of this process can be visualized in figure 4.

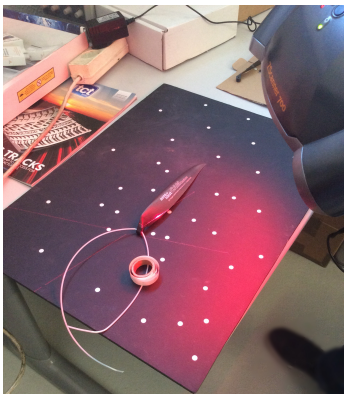

Figure 4: 3D scanning measurement of the blade

However, this method showed to be very inaccurate, due to the imprecision of the measuring laser system used and, as so, the measurements obtained by the first method were used in the initial simulations on this thesis.

To predict the performance of a propeller, it was also necessary to determine the airfoil parameters. Knowing that the airfoils used were the Clark-Y or the NACA 4412 [8], the parameters of each one were calculated using the software XFOIL. To calculate the Reynolds number to set in the analysis, it was considered that

$$Re = \frac{\rho \Omega R c_{avg}}{\mu} \, , \tag{13}$$

where c_{avg} is the arithmetic mean of the chord values of each section, for each propeller and μ is the kinematic viscosity. It was expected in this phase that all systems could reach a rotation speed of 5000 RPM, which corresponds to 533.33 rad/s, without damaging the motor. As such, the data obtained for each propeller is presented in Table 2.

Propeller	$c_{avg}\,[mm]$	R $[mm]$	Re
APC 13”×8”	17.47	145	94416
APC 16”×8”	20.37	183	138908
APC 16”×10”	21.15	180.2	142073

Table 2: Determination of Reynolds number

Since it was desired to set an unique Reynolds number for all propellers, it was decided to set $Re = 100000$ due to this value being a good approximation of all the tested cases. The resulting graphics with polar curves for each airfoil can be visualized in Figure 5.

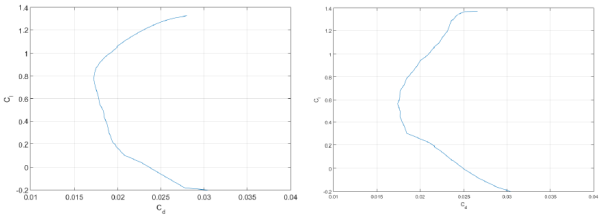

(a) Clark-Y (b) NACA 4412

Figure 5: Polars from the different possible airfoils in use

From the graphics presented in Figure 5, all the variables necessary to define the polar curve of each airfoil were determined. At the end, the propeller files were totally defined.

4.3. Force Balance

To obtain the desired data for the determination of the parameters of the propeller, it is necessary to perform static and dynamic tests in the wind tunnel, using a force balance to support the system motor+propeller and the sensors used to measure the parameters. According to [9], the construction of the balance was divided in several stages, which are presented in the diagram of Figure 6:

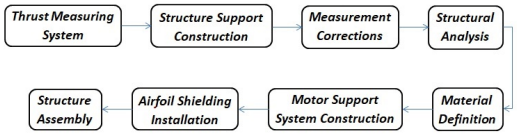

Figure 6: Diagram with the several stages of construction of the balance

For the design of the connection between the motor and the propeller, some changes had to be done since the previous support was over-sized. The balance was initially designed with the capability to test propellers up to 27” of diameter that could generate a force equivalent to 30 kgf. Using the method present in [10], it was concluded that the best option would be to replace the existing M10 bolts by M4 bolts of Steel AISI 1035HR, which would still provide a safety factor of 32. To build the structural crosses it was used a 3D Printing process using PLA as construction material. The structural plates were replaced by new ones made of acrylic, whose holes were made using a drilling process. It is possible to observe the new measuring system in Figure 7.

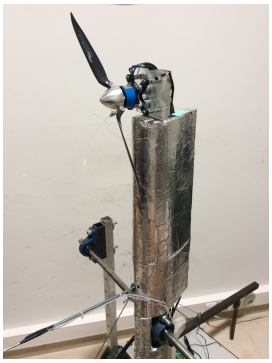

Figure 7: Resized support of the system motor+propeller

To enable the measurement of the necessary data to analyse the performance of the motor and the propeller, it was necessary to mount sensors installed in the structure. To measure the loads applied in the system, two different load cells were used, according with the system motor+propeller in use. To assure the accuracy of the values detected by the sensor, each load cell had to be calibrated. The graphics resulting of the linear regressions used in the calibration process are presented in Figure 8.

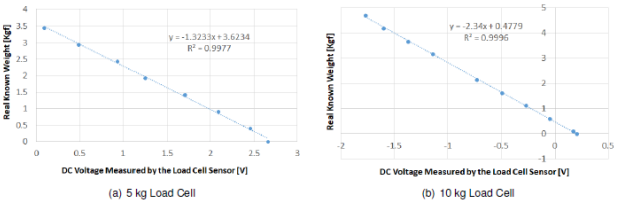

(a) 5 kg Load Cell (b) 10 kg Load Cell

Figure 8: Linear regressions used to calibrate the load cell sensors

To measure the voltage and the current in the motor, two equal sensors were used, one to measure each parameter. To calibrate both electrical sensors responsible to measure voltage and current, two different tests were conducted. To calibrate the voltage sensor, it was used a multimeter connected to a variable power supply. The current calibration was performed by increasing the thrust level. The graphics with the linear regressions resulting of the calibrations of the sensor for each motor are presented in Figures 9 and 10.

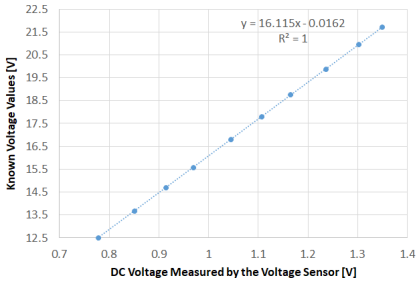

Figure 9: Linear regressions used to calibrate the voltage sensor with the OS-5020-490

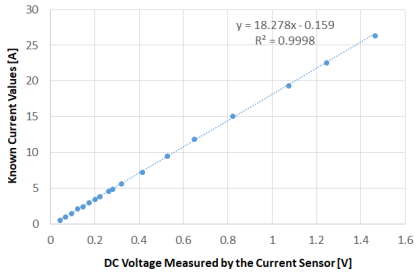

Figure 10: Linear regressions used to calibrate the current sensor

To measure the airspeed, two sensors were used: the first one to measure the static pressure and the second one to measure the total pressure. With these two values of pressure, the software obtained the airspeed value using Bernoulli equation,

$$U = \sqrt{\frac{2\left(P^*_{tot} - P^*_{static}\right)}{\rho}}\,. \tag{14}$$

Knowing the values of the dynamic pressure and using a linear regression, it was determined the relation between the dynamic pressure and the voltage values measured by the sensor connected to the pitot tube placed at the balance. The graphic obtained from this linear regression is shown in Figure 11.

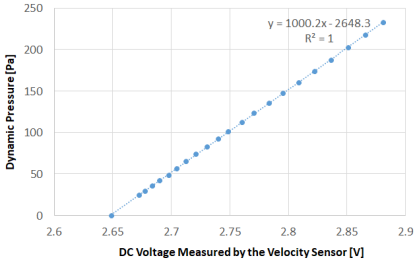

Figure 11: Linear regression used in the calibration of the airspeed sensor

The value of density ρ corresponded to the value calculated for the day when the tests were performed. Sensors to measure the RPM, the airstream and motor temperature were also used and were all connected to a Data Acquisition System (DAQ).

5. Initial Propeller Analysis

After preparing the experimental facility, the experimental tests were performed, using the force balance previously described and the software LabView® Interface User, inside the wind tunnel, where it was possible to assure a laminar flow. In these tests, several parameters were analysed for each combination of motor+propeller, for different electrical conditions, in particular thrust, electrical power, thrust coefficient, power coefficient and efficiency.

5.1. LEEUAV Case Study

After performing the experimental tests, it was analysed the best way to apply its results to the case in study, the LEEUAV. In [11], several flight tests were performed in cruise conditions, which is the stage of flight where the UAV spends more time, which allowed to determine the value of required thrust for a given airspeed. Since the efficiency for each airspeed and thrust was determined in the experimental tests, it was possible to analyse the propeller efficiency variation of a given system by applying the LEEUAV cruise flight conditions. This process was important since it was possible, before any optimization, to verify which system would be more efficient to apply in the LEEUAV. The parameters taken in account in this analysis were the propeller diameter, the propeller pitch, the electrical motor and the input voltage. The experimental propeller efficiency variation for each system obtained for cruise conditions is shown in figure 12.

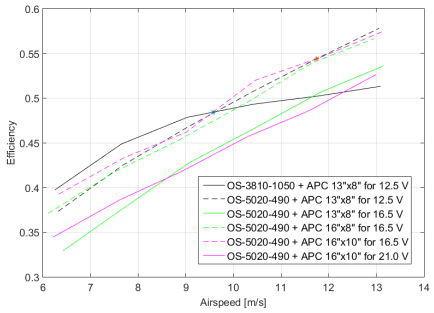

Figure 12: Comparison of the variation of efficiency with airspeed for all systems

So, it is possible to conclude from the analysis of Figure 12 that: the motor OS-3810-1050 is the most efficient for velocities below 9.57 m/s; the higher the diameter, the higher the efficiency; the higher the pitch, the higher efficiency and the higher the input voltage on a given system motor+propeller, the lower the efficiency.

Since the LEEUAV at cruise conditions travels at an airspeed of 7.53 m/s, the most efficient system to implement would be the OS-3810-1050 + APC 13"×8" for 12.5 V. Besides the efficiency, it was also analized the variation of the thrust coefficient C_T and the power coefficient C_P with the advance ratio J and compared with the literature results obtained from [12], as it is presented in Figures 13 and 14.

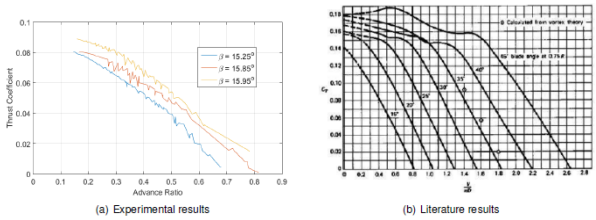

(a) Experimental results (b) Literature results

Figure 13: Variation of thrust coefficient with advance ratio

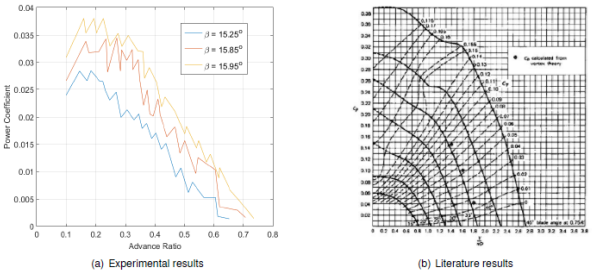

(a) Experimental results (b) Literature results

Figure 14: Variation of power coefficient with advance ratio

As it is shown in Figures 13 and 14, both coefficients decrease with the increase of the advance ratio that although the curves exhibit similar behaviour, the experimental values are lower relatively to the literature, which means that the calculated blade angles were higher than the real ones.

5.2. Analysis Framework and Validation Procedure

To obtain the simulations data, a routine in MATLAB®, called "Analysis Framework" was developed with the objective of facilitating the construction of the optimizer, allowing the user to insert the necessary inputs and then to present the outputs, as schematically shown in Figure 15.

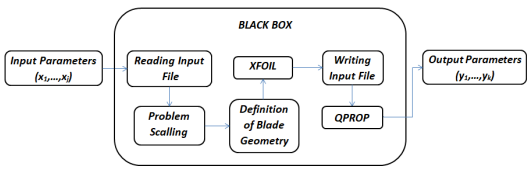

Figure 15: Analysis framework used to make the simulations

After obtaining the experimental results, it was possible to compute the numerical results using the software QPROP. However, at this stage, it was important to assure the highest level of accuracy of the numerical software due to the intention of using it later in the optimization process. As such, to perform the validation, it was used the *Least Squares Fitting* method [13]. With this method, a residual is generated and is given by

$$Residual = \sum \left(y_{exp} - y_{num}\right)^2 . \qquad (15)$$

The parameters that were used in the validation were the offset add to the β distribution of the blades, β_{add}, due to be the one subjected to higher errors, since it was calculated using manual measurement and to affect the numerical thrust results and the internal resistance of the motor R due to affecting the electrical power results. The validated results obtained in this validation are presented in Tables 3 and 4.

Propeller	Airfoil	β_{add} [°]
13"×8"	NACA 4412	0.58
16"×8"	Clark-Y	−0.5
16"×10"	Clark-Y	−1.07

Table 3: Summary table with the validated characteristics for each propeller

Motor	Resistance [$m\Omega$]
OS-3810-1050	75.9
OS-5020-490	88.5

Table 4: Summary table with the validated internal resistance for each motor

6. Propeller Optimization

6.1. Process Description

Before using any kind of optimization algorithm, it is necessary to define the problem and what is desired to be optimized. An optimization problem is composed by an objective function, the design variables and it can have bound constraints, linear and non-linear constraints. After analysing which were the parameters that would have a better impact on the propeller performance, it was decided that the objective of the optimization problem was to optimize the propeller efficiency, (7).

However, it was desired to optimize the efficiency for both flight stages, so, two different functions were created: η_{cruise} and η_{climb} which correspond to the propeller efficiency for cruise and climb condition, respectively. Since it was only intended to generate one optimum propeller, a final objective

function was created, η_{total} that corresponds to efficiency of the entire flight.

The system used as a starting point in this process was the OS-3810-1050 + APC 13"×8" with the NACA 4412 airfoil since this motor was already installed in the LEEUAV. The optimization process was performed for climb and cruise conditions considering airspeeds of 7.67 m/s and 7.53 m/s, respectively. A flowchart describing the entire optimization process is presented in Figure 16.

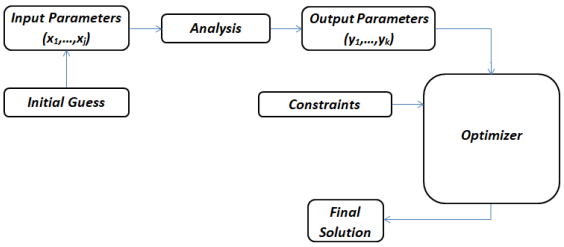

Figure 16: Optimization process scheme

To perform the optimization, it was used the the *Interior-Point* algorithm due to be a deterministic gradient-based constrained numerical method. This type of method was used since the initial data was known accurately, the studied parameters functions presented a smooth behaviour and due to the existence of bound and nonlinear constraints.

6.2. Geometry Optimization

Because QPROP only exports discrete results, a relative step size factor was set to define the initial step in finite differences approximations to the function gradients. To define this variable, a study to the variation of the derivative of the objective function in a given point in order to different design variables with the finite differences was performed.

To perform the propeller optimization, it was used a multi-objective optimization with the weighted aggregation method described in [14]. In this work, it is desired to optimize the cruise and climb efficiencies, however, a propeller optimized for a unique flight condition is less efficient for the other one. In this case, it was decided to define the weight ϵ as

$$\epsilon = \frac{E_{cruise}}{E_{cruise} + E_{climb}}\,, \tag{16}$$

where E_{cruise} is the total energy spent by the UAV in cruise and E_{climb} is total energy spent by the UAV during the climb. According to [15], the required energy during climb is 266.9 kJ and the required energy during cruise is 1370.9 kJ, which means that $\epsilon = 0.837$. As such, it was possible to build the objective problem as

$$\eta_{total} = 0.837\eta_{cruise} + 0.163\eta_{climb}\,, \tag{17}$$

The optimization problem is defined as:

$$\begin{aligned}
\text{Maximize} \quad & \eta_{total} = F(\vec{x}_{total}) \\
\text{w.r.t.} \quad & \vec{x}_{total} = (\beta_1, \beta_2, \beta_3, \beta_4, c_1, c_2, c_3, \\
& c_4, R, RPM_{cruise}, RPM_{climb}) \\
\text{subject to} \quad & \vec{x_0}_{total} = (90, 23, 14, 0.3, 7, 24, 13, \\
& 1.2, 150, 3550, 6250) \\
& \vec{lb}_{total} = [87, 22, 13, 0, 6, 22, 12, \\
& 1, 145, 3500, 6200] \\
& \vec{ub}_{total} = [90, 24, 15, 0.5, 9, 25, 15, \\
& 2.1, 184, 3700, 6400]
\end{aligned} \tag{18}$$

where $\vec{x}_{total}$ is the design variables vector, $\vec{x_0}_{total}$ is the initial guess of the design variables vector, $\vec{lb}_{total}$ and $\vec{ub}_{total}$ are the lower and upper bound constraints, respectively, R is the propeller radius, RPM_{cruise} and RPM_{climb} are the RPM for cruise and climb conditions, respectively, R is the propeller radius and $\beta_1, \beta_2, \beta_3\beta_4, c_1, c_2, c_3, c_4$ are the four equidistant points used to build the cubic spline for $\beta(r)$ and $c(r)$ distributions respectively, as shown in Figure 17.

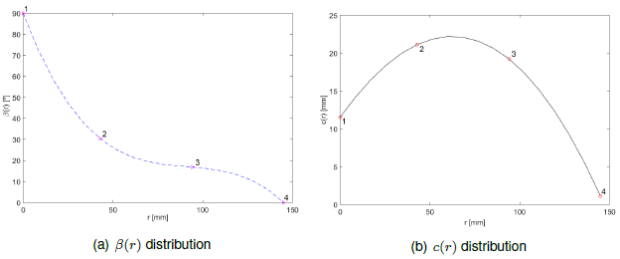

(a) $\beta(r)$ distribution (b) $c(r)$ distribution

Figure 17: Optimization process scheme

According with the results obtained from Figure 12, it was possible to verify that for the cruise, a minimum value for thrust of 3.57 N was obtained. For climb conditions, it was obtained a minimum value of thrust of 13.88 N. Since for an input voltage of 12.5 V, it was only possible to obtain a maximum current of 30 A to perform in total secure conditions, it was decided to limit the maximum electrical power of the motor to 375 W. Consequently, to assure that these requirements were fulfilled, it was necessary to apply a nonlinear constraint in the form:

$$\begin{aligned}
C_1 &= 3.57 - T \\
C_2 &= 13.88 - T \\
C_3 &= P - 375 \\
C_{eq} &= [\,]\,.
\end{aligned} \tag{19}$$

After performing the optimization of this problem, it was determined that the optimum blade ra-

dius, R, was 168.52 mm. In figure 18, it is possible to visualize in figures 18 and 19, the $c(r)$ and $\beta(r)$ distributions comparison between the initial and the optimum propeller.

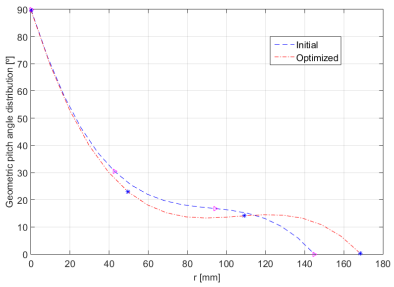

Figure 18: Geometric pitch angle distribution of the propeller blades before and after the optimization

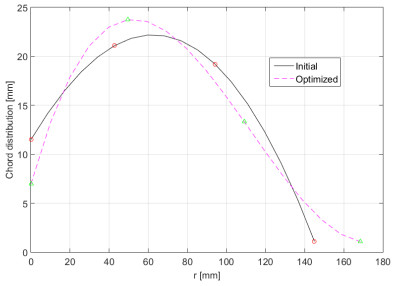

Figure 19: Chord distributions propeller blades before and after the optimization

The results between the performance of the initial propeller and the final propeller are presented in table 5.

Flight Stage	U $[m/s]$	RPM	T $[N]$	C_T	C_P	J	P $[W]$	η[%]
Climb - initial	7.67	5934	13.88	0.0867	0.0433	0.2301	375.2	28.38
Climb - final	7.67	6270	13.88	0.0462	0.0185	0.218	344.1	30.94
Cruise - initial	7.53	3317	3.57	0.0714	0.0435	0.4042	59.36	45.28
Cruise - final	7.53	3610	3.57	0.036	0.018	0.371	58.77	45.76

Table 5: Comparison of the results obtained for the initial and the final propeller

At the end, it was possible to compare the total efficiencies of the flight for the initial and the optimized propeller. For the initial propeller, a total efficiency $\eta_{total} = 42.53\,\%$ was obtained and for the optimized propeller, a total efficiency of $\eta_{total} = 43.34\,\%$ was obtained. With this optimization, a value of 244.8 kJ is obtained for climb conditions and a value of 1356.52 kJ is obtained for cruise conditions, which results in an increasing of 9 minutes of flight time.

6.3. 3D Optimal Design

After the optimization process being completed, a new propeller file was obtained with the detailed geometry distribution parameters. Initially, to design a tridimensional model, it was necessary to determinate the coordinates of the points for a n-section. This points are calculated according to

$$\begin{bmatrix} \vec{x_k^*} \\ \vec{y_k^*} \end{bmatrix} = c_k \times \begin{bmatrix} \cos\beta_k & \sin\beta \\ -\sin\beta_k & \cos\beta_k \end{bmatrix} \times \begin{bmatrix} \vec{x_k} \\ \vec{y_k} \end{bmatrix} \quad (20)$$

where $\vec{x_k}$ and $\vec{y_k}$ are the vectors of coordinates of the original profile, $\vec{x_k^*}$ and $\vec{y_k^*}$ are the new coordinates of the airfoil for each section of the blade and c_k is the chord value for each section. After having all the points on the rotated referential for each section, a tridimensional model of the propeller was designed using the software SOLIDWORKS®. After modelling the blade, the model was printed in PLA, with a filament diameter of 0.4 mm, using a 3D-printer. The physical model of the optimized blades can be visualized in figure 20.

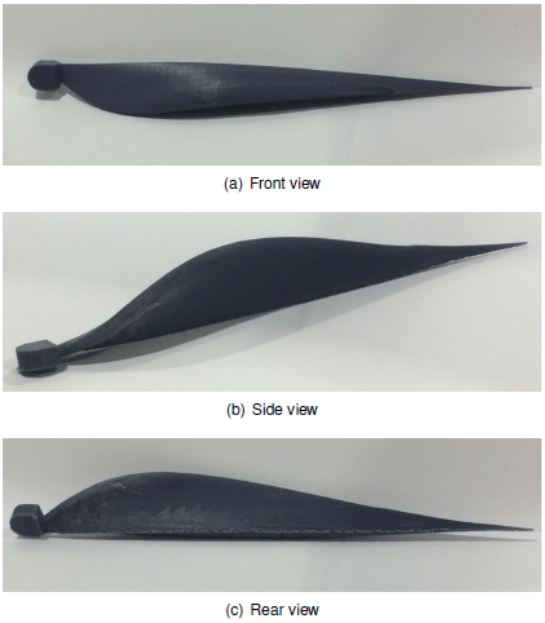

Figure 20: Rotated views of the physical three-dimensional model

7. Conclusions

Despite the existing of several numerical softwares to perform propulsive numerical analysis, the best choice was QPROP, since it was the only one that takes in account the characteristics of the complete system and allowed both an initial analysis and a posterior use in the optimization process.

Since it was pretended to optimize the propeller efficiency by reducing the electrical power consumed by the system, it was concluded that the best option was to define this parameter as the ratio between the power that a propeller can use and the electrical power supplied to the system.

When the propeller measurements were performed, it was verified that the results obtained

from the manual measurements were more accurate than the results obtained from the 3D scanning method. To determine the airfoil characteristics, it was decided to use $Re = 100000$, since this value would be a good approximation for the tested cases. To perform the experimental tests, the motor support system had to be changed since the previous one was oversized, which could lead to additional drag that could affect the experiments. As such, it was concluded that the best option would be to replace the existing M10 bolts by M4 bolts of Steel AISI 1035HR, which would still provide a safety factor of 32.

After performing the experimental tests and applying the gathered data to the specific case of the LEEUAV, it was concluded that the use of the motor OS-3810-1050 was more efficient for airspeeds below 9.57 m/s; the higher the diameter and the pitch of a propeller, the higher the efficiency and that the efficiency decreases with the increase of the input voltage. It was also concluded that the distribution of the geometric pitch angle distribution obtained from the manual measuring was overestimated in the three tested propellers. To validate the propellers, the parameter β_{add} was used since this was the parameter most sensible to uncertainties. To validate the motor, the internal resistance of the motor R was used as a parameter.

Since it was only intended to produce a single propeller, a multi-objective optimization using the weighted aggregation method was performed, where a single propeller optimized for both flight conditions was obtained. With the optimization process, it was verified an increasing of the propeller efficiency for both flight stages, which resulted in an increase of the total efficiency of the flight. At the end, the new blade was projected using the software SOLIDWORKS® and a physical model was printed in PLA, with a diameter filament of 0.4 mm, using the rapid prototyping method.

References

[1] Luís Miguel Almodôvar Parada. Conceptual and Preliminary Design of a Long endurance Electric UAV. Master's thesis, Instituto Superior Tcnico, November 2016.

[2] Jan Roskam. *Airplane Aerodynamics and Performace*. DARcorporation, 1^{st} edition, 1997. ISBN: 1-884885-44-6.

[3] Mark Drela. QPROP formulation. `http://web.mit.edu/drela/Public/web/qprop/qprop_theory.pdf`, June 2006.

[4] Aage Berg. AKPD/AKPA. `https://www.sintef.no/globalassets/upload/marintek/pdf-filer/sofware/akpd-akpa_programpackage.pdf` accessed on Mar 2017.

[5] Martin Hepperle. JavaProp - Users Guide. `http://www.mh-aerotools.de/airfoils/javaprop.htm` accessed on Mar 2017.

[6] O.S. Engine. `https://www.osengines.com/` accessed on Feb 2018.

[7] Sara Santos, Bruno Soares, Marco Leite, and Jorge Jacinto. Design and development of a customised knee positioning orthosis using low cost 3D printers. *Virtual and Physical Prototyping*, March 2017. doi: 10.1080/17452759.2017.1350552.

[8] APC Propellers. `https://www.apcprop.com/Articles.asp?ID=262#airfoil` accessed on May 2017.

[9] Miguel Borges. Design of an Apparatus for Wind Tunnel Tests of Electric UAV Propulsion Systems. Master's thesis, Instituto Superior Tcnico, June 2015.

[10] Richard G. Budynas and J. Keith Nisbett. *Shigley's Mechanical Engineering Design*. McGraw-Hill Education, 10^{th} edition, 2015. ISBN:978-981-4595-28-5.

[11] Afonso Rodrigues. Airframe Assembly, Systems Integration and Flight Testing of a Long Endurance Electric UAV. Master's thesis, Universidade da Beira Interior, February 2017.

[12] Barnes W. McCormick. *Aerodynamics Aeronautics and Flight Mechanics*. Pennsylvania State University, 2^{nd} edition, April 1995. ISBN:0-471-5706-2.

[13] P. R. Bevington. *Data Reduction and Error Analysis for the Physical Sciences*. McGraw-Hill, New York, 1969. ISBN: 0-07-247227-8.

[14] Patrick Ngatchou, Anahita Zarei, and M. A. El-Sharkawi. Pareto Multi Objective Optimization. *Intelligent Systems Application to Power Systems*, pages 84–89, 2005. doi: 10.1109/ISAP.2005.1599245.

[15] André C. Marta and Pedro V. Gamboa. Long Endurance Electric UAV for Civilian Surveillance Missions. 29^{th} *Congress of International Council of the Aeronautical Sciences*, September 2014.